Korea-Australia Rheology Journal
Vol. 16, No. 2, June 2004 pp. 75-83

Numerical simulations of fluid mechanical interactions between two abdominal aortic branches

Taedong Kim, Taewon Seo*[1,2] and Abdul.I. Barakat[2]
Dept. of Environmental Eng., Andong National University, Andong 760-749, Korea
[1]School of Mechanical Eng., Andong National University, Andong 760-749, Korea
[2]Dept. of Mechanical and Aeronautical Eng., University of California, Davis, CA 95616, USA
(Received November 17, 2003; final revision received March 8, 2004)

Abstract

The purpose of the present study is to investigate fluid mechanical interactions between two major abdominal aortic branches under both steady and pulsatile flow conditions. Two model branching systems are considered: two branches emerging off the same side of the aorta (model 1) and two branches emerging off the opposite sides of the aorta (model 2). At higher Reynolds numbers, the velocity profiles within the branches in model 1 are M-shaped due to the strong skewness, while the loss of momentum in model 2 due to turning effects at the first branch leads to the absence of a reversed flow region at the entrance of the second branch. The wall shear stresses are considerably higher along the anterior wall of the abdominal aorta than along the posterior wall, opposite the celiac-superior mesenteric arteries. The wall shear stresses are higher in the immediate vicinity of the daughter branches. The peak wall shear stress in model 2 is considerably lower than that in the model 1. Although quantitative comparisons of our results with the physiological data have not been possible, our results provide useful information for the localization of early atherosclerotic lesions.

Keywords : aortic branch, fluid mechanical interactions, pulsatile flow, atherosclerosis

1. Introduction

Atherosclerotic lesions appear most frequently in regions of arterial branches and curvatures of medium to large arteries. It is common knowledge that the local flow disturbances due to the presence of an arterial branch where secondary flows and vortices develop play a significant role in the localization of early atherosclerotic lesions and the further development of atherosclerosis (Karino *et al.*, 1979; Lei *et al.*, 1995). In the presence of a single branch the importance of arterial flow characteristics such as flow separation, secondary flow and particle residence time to atherogenesis has become increasingly evident (Cheer *et al.*, 1998; Shipkowitz *et al.*, 2000). Computational studies have demonstrated that the flow field is affected by the complex three-dimensional geometry of both the parent vessel and its branches (Taylor *et al.*, 1998; Buchanan *et al.*, 2003). The flow field in the abdominal aorta with the left and right renal arteries is considerably more disturbed in rabbits exhibiting small spacing between these two branches (Barakat *et al.*, 1997a). Their study has shown that the fluid mechanical interactions between arterial branches depend on the distances among the branches and their relative orientations as well as on the various geometric and flow parameters that govern flow disturbance in the presence of arterial branch and curvature.

Despite recent computational studies of multi-branch arterial flow geometries, the physics of branch-branch interactions remain incompletely understood. The purpose of the present computational study is to investigate fluid mechanical interactions between two large arterial branches that model major abdominal aortic branches under both steady and pulsatile flow conditions. Our attention will be focused on the dependence of branch-branch interactions on the Reynolds number, on the distance between the branches, and on the relative orientation of the branches. Although the physiological relevance of this study due to the assumption of flow conditions is limited, the results presented in this study provide insight into the fundamental fluid mechanical interactions between two abdominal aortic branches.

2. Computational model

The fraction of the flow rate into the branches in the aorta is important when consider the physiologic function and the drug delivery. The flow field due to the flow division in the branches and aorta is affected significantly and the details of the flow field have been assumed to play an

*Corresponding author: dongjin@andong.ac.kr
© 2004 by The Korean Society of Rheology

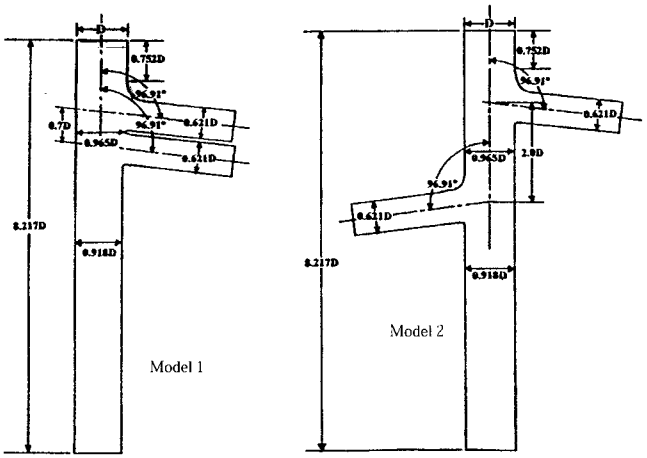

Fig. 1. The schematic diagrams of the abdominal aorta and branches in the common median plane.

important role as the early atherosclerotic lesions. According to the measurements of flow rates through aortic branches in the rabbit (*Barakat et al.*, 1997b), the approximately 60% of the flow rate in the steady and pulsatile flows divides into the celiac and cranial mesenteric arteries. Barakat *et al.* (1997b) found from the measurement of flow rate through the aortic branch in a rabbit that the flow rate through the cranial mesenteric artery was the highest (averaging 32% of the total), and the next was in the celiac artery (25.6%).

Two different models of abdominal aortic branches in the rabbit are examined under both steady and pulsatile flow conditions. The two models differ in daughter branch positions as well as in the distance between the branching points as depicted schematically in Fig. 1. Model 1 is representative of a celiac-superior mesenteric artery configuration, while model 2 might simulate the region of the right and left renal arteries. The models are fully three-dimensional, and the cross-sections of the parent vessel and the branches are assumed circular. The diameter D of the mother vessel of each model represents the abdominal aortic diameter of a rabbit and has a value of 4.25 mm in the geometric models. As shown in Fig. 1, the lengths of the abdominal aorta upstream and downstream of the branches (celiac artery) are 0.752 and 6.223 aortic diameters, respectively. The branches are 2.25 aortic diameters long. As shown in Fig. 1, the celiac artery branches off the abdominal aorta at an angle of 96.91°, and the diameter of the celiac artery branches to the abdominal aorta at the flow inlet is 0.621D. Downstream of the abdominal aorta has 0.918 aortic diameter of the flow inlet.

Blood is treated as an incompressible, homogeneous, Newtonian fluid and the arterial wall is assumed to be rigid. Under these assumptions the flow through the model can be described using the non-dimensionalized Navier-Stokes and continuity equations:

$$\nabla \cdot \vec{u} = 0 \tag{1}$$

$$\frac{1}{2\pi Re}\frac{\alpha^2 \partial \vec{u}}{\partial t} + (\vec{u} \cdot \nabla)\vec{u} = -\nabla p + \frac{1}{Re}\nabla^2 \vec{u} \tag{2}$$

where ρ is the blood density, $\vec{u}$ and p are the velocity vector and pressure, respectively. The Reynolds number, Re, based on the abdominal aortic diameter at the inlet (D) and mean axial velocity (U_m) at the aortic flow and the Womersley parameter, α, are defined as

$$Re = \frac{U_m D}{\nu}, \quad \alpha = \frac{D}{2}\sqrt{\frac{2\pi}{\nu T}} \tag{3}$$

where ν is the kinematic viscosity of blood, and T is the pulsatile flow period.

The Newtonian approximation for blood is acceptable in modeling flow in large arteries. However, it has been observed that blood behaves as Non-Newtonian fluid at the very small shear rates in the regions of flow separation and recirculation, and in vessel of small diameter. Seo *et al.* (2004) demonstrated the primary impact of the Non-Newtonian effect is to reduce to size of the flow separation region downstream of stent by approximately 8% in large artery.

For the steady flow simulations, two types of boundary conditions are prescribed at the inlet of the abdominal aorta.

- Parabolic velocity profile; $u = U_{max}\left(1 - \frac{r^2}{R^2}\right)$
- Uniform velocity profile; $u = U_m$

For the pulsatile flow simulations, the inlet velocity is assumed to be uniform with a sinusoidal temporal waveform;

- $u = U_m(1 + \sin 2\pi t)$

At the outlet, flow satisfies the fully developed flow conditions. The lengths of the daughter branches were chosen to be sufficiently long to satisfy this outlet condition. The velocity boundary conditions are either parabolic or uniform profile at the aortic inlet, 30% of the total at each branch outlet consistent with the *in vivo* experimental findings (*Barakat et al.*, 1997b), and zero pressure at aortic outlet. A no-slip condition is imposed at the wall.

The simulations were performed to two different geometries and various flow parameters in order to assess the sensitivity of the flow field. The aortic inlet velocity profiles are uniform, parabolic and the pulsatile flow and the Reynolds numbers of 200, 500, 800, and 1200.

The solution of the governing Navier-Stokes equations for the three-dimensional geometries modeled is obtained using the commercially available CFD code FLUENT. In FLUENT the momentum is discretized using a second order upwind scheme. The pressure-velocity coupling is accomplished through the SIMPLEC scheme. Unstruc-

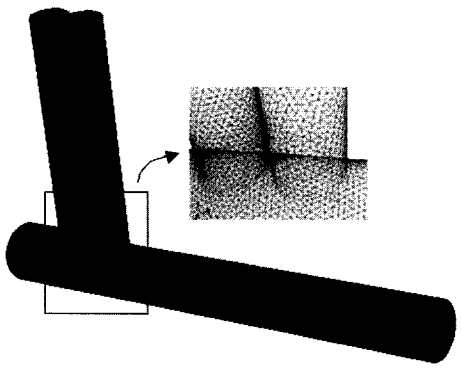

(a) Model 1

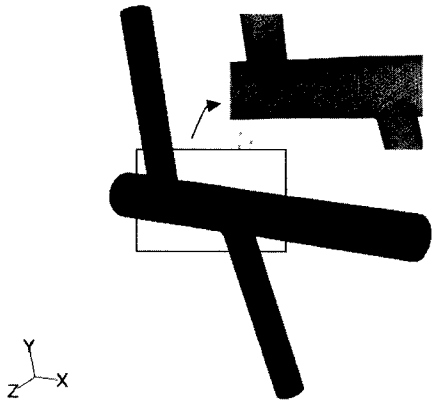

(b) Model 2

Fig. 2. Computational meshes used in models.

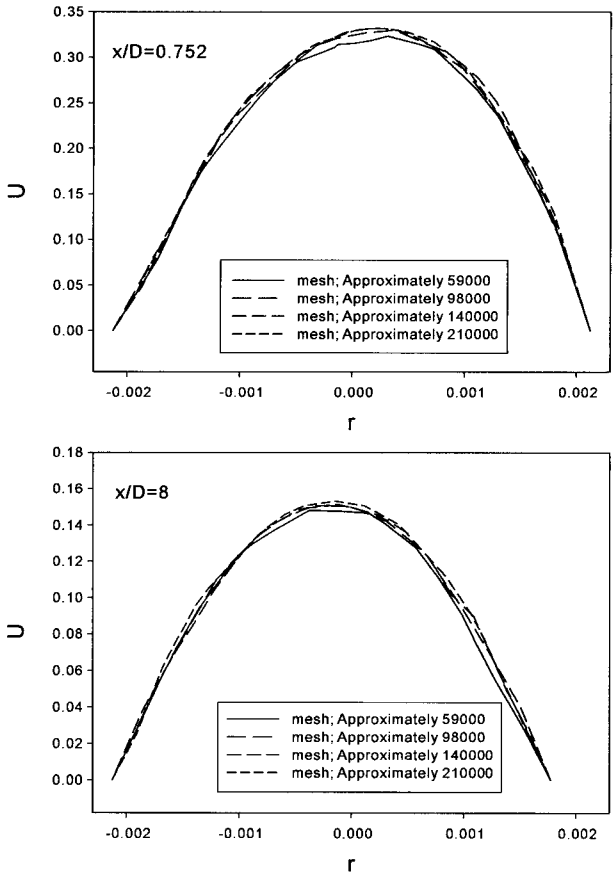

Fig. 3. Mesh independence.

tured meshes with 213,858 tetrahedral cells given in Fig. 2 were used in both model 1 and 2. All the computations were performed on an Intel Pentium III 1.2 GHz, with 1 GB RAM operating Windows XP. The computational run times ranged from approximately 5 hours for the simplest steady flow runs to several days for the pulsatile flow simulations.

3. Results

Mesh independence was investigated for model 1 in Fig. 3 by comparing distributions of axial velocities at two different locations in which one is just before the first branch located $x/D = 0.752$ and the other is far downstream along the mother vessel ($x/D = 8$) with approximately 59000, 98000, 140,000, and 210,000 nodes, respectively. Simulation results were assumed to be independent of the computational mesh when the disparity between meshes of varying densities was less than 5%. In pulsatile flow, convergence for each time step was based on the residual in continuity falling below a prescribed value (typically 10^{-5}). Time periodic solutions were typically obtained within 4~5 cycles and were defined when the cycle average difference in the size of the flow separation zone in the vicinity of the daughter branches between two successive cycles fell below 5%. Under those conditions, differences in velocities between successive cycles were smaller than 1%.

Simulations for Reynolds numbers (based on inlet aortic diameter and mean inlet velocity) of 200, 500, 800, and 1200 were performed. For steady flow in model 1, the results in Fig. 4 show the velocity profiles at the entrance of both the daughter branches are skewed toward the distal wall of the bifurcations due to the curvature. These profiles shift gradually toward the centerline as the flow proceeds. The flow in the daughter branches becomes fully developed at the outlet for Reynolds numbers of 200 and 500, while the flow remains skewed for Reynolds numbers of 800 and 1200.

Fig. 5 depicts the dependence of the regions of the flow separation and recirculation zone in the immediate vicinity of the daughter branches in model 1. As shown in Fig. 5, regions of low flow velocity are present along the proximal wall of the daughter branches and in the mother vessel along the wall opposite the daughter branches. The low flow velocity occupies approximately 60% of the cross-sectional area of the daughter branches for Reynolds numbers 800 and 1200. As a result, the velocity profiles within the daughter branches for Reynolds numbers 800 and 1200

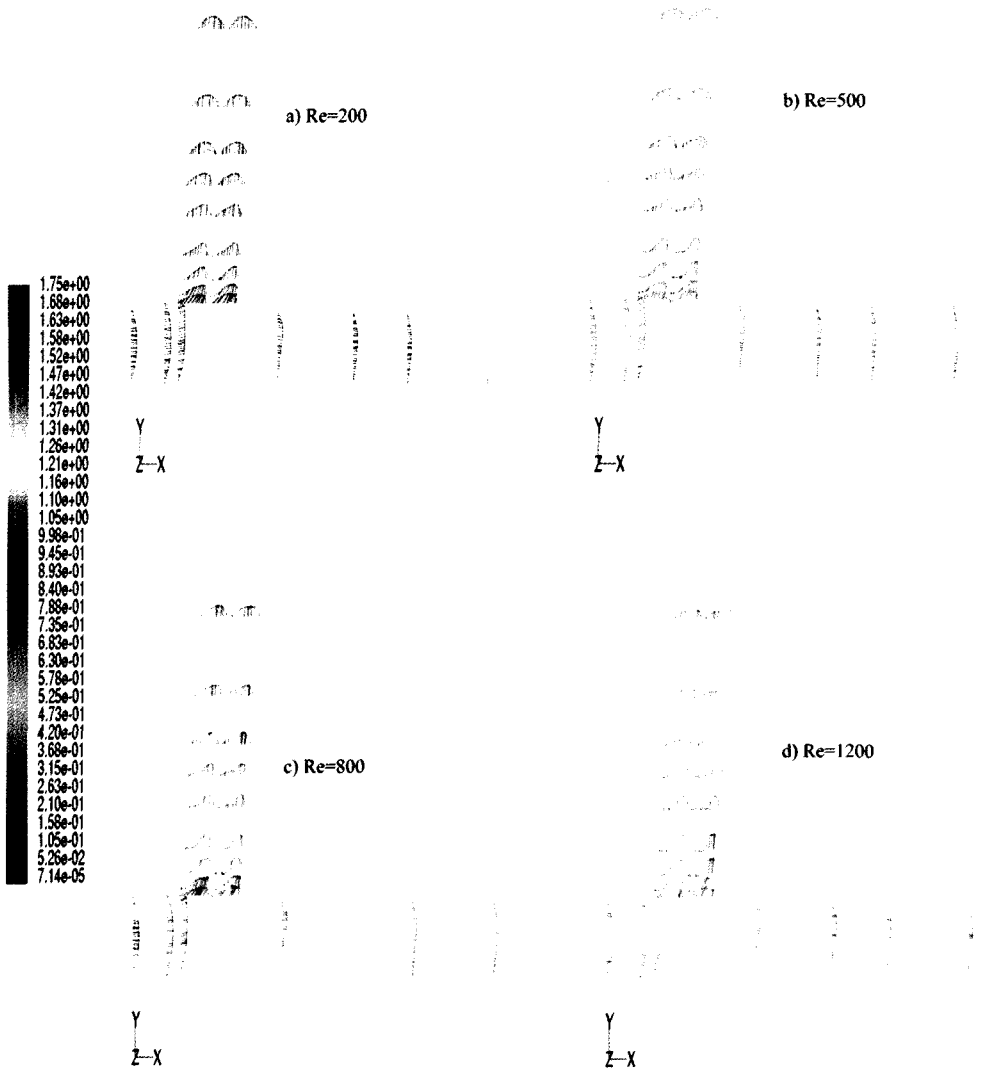

Fig. 4. The velocity magnitude vectors for Reynolds numbers 200, 500, 800, and 1200 in model 1.

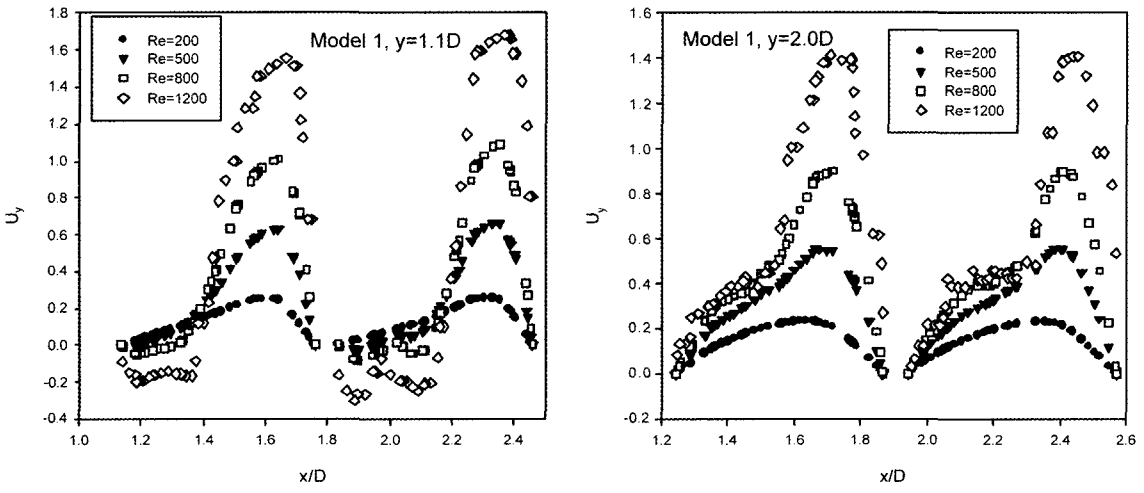

Fig. 5. The streamwise velocities in the daughter branches at y = 1.1*D* and 2.0*D* in model 1.

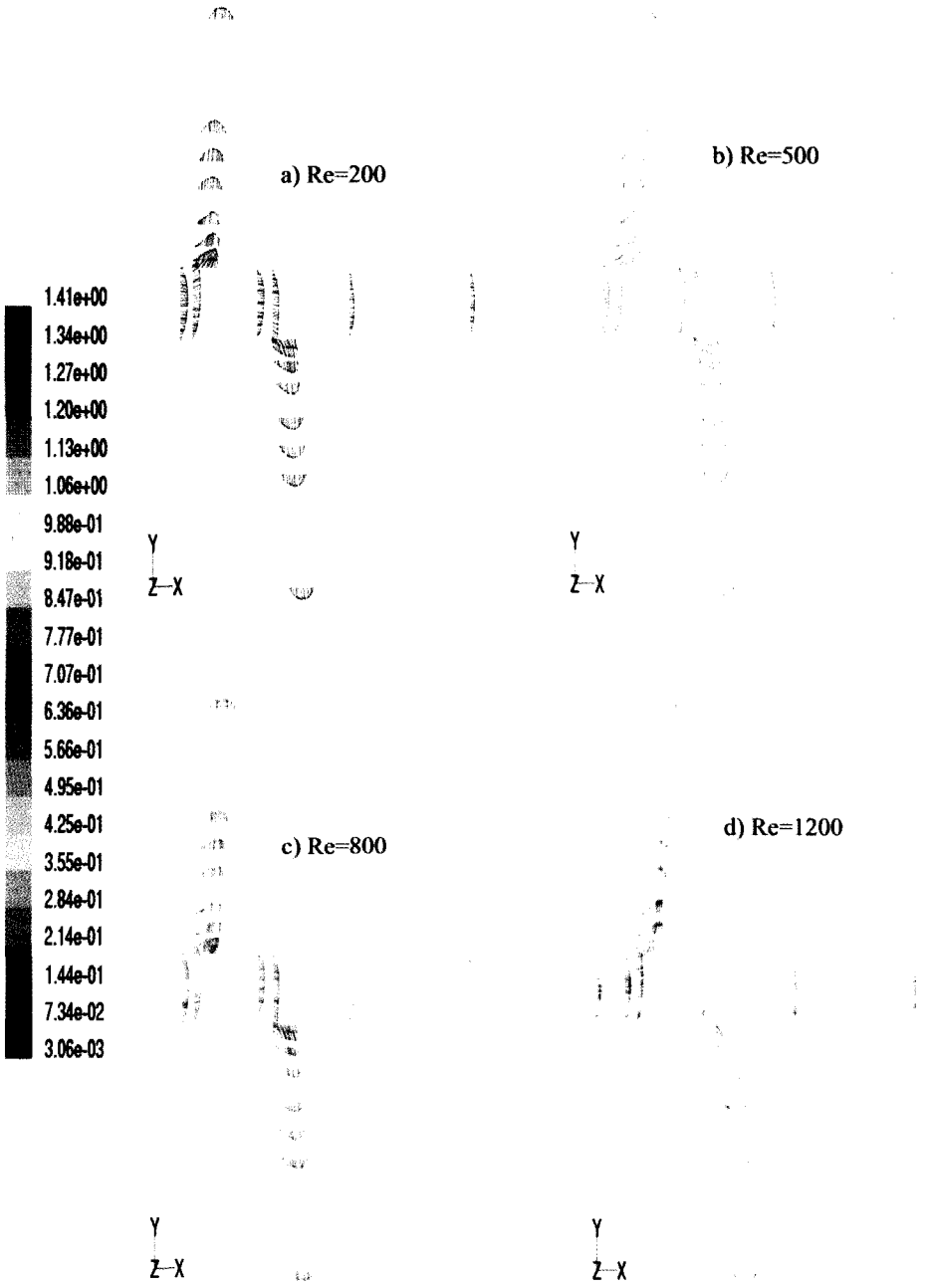

Fig. 6. The velocity magnitude vectors for Reynolds numbers 200, 500, 800, and 1200 in model 2.

are M-shaped due to the strong skewness of the velocity profiles. It is noted that the size of the recirculation region in the second branch is considerably larger than in the first branch due to the strong centrifugal effect of the flow for Re = 1200.

For steady flow in model 2, Fig. 6 shows that, similar to model 1, the flow in the mother vessel shifts towards the first branch, and the velocity profiles in the entrance region of the branch are skewed toward the distal wall of the bifurcation due to the curvature. However, at a Reynolds number of 1200, the reverse flow only occupies approximately 30% of the cross-sectional area of the first daughter branch. As the flow proceeds downstream in the mother vessel, the direction of the flow shifts to the opposite side. Loss of momentum due to turning leads to the absence of a reversed flow region at the entrance region in the second branch.

Fig. 7 illustrates the reverse flow region at the positions of $y = \pm 1.1D$ and $\pm 2.0D$. The velocity shifts toward the posterior wall of the mother vessel due to the presence of

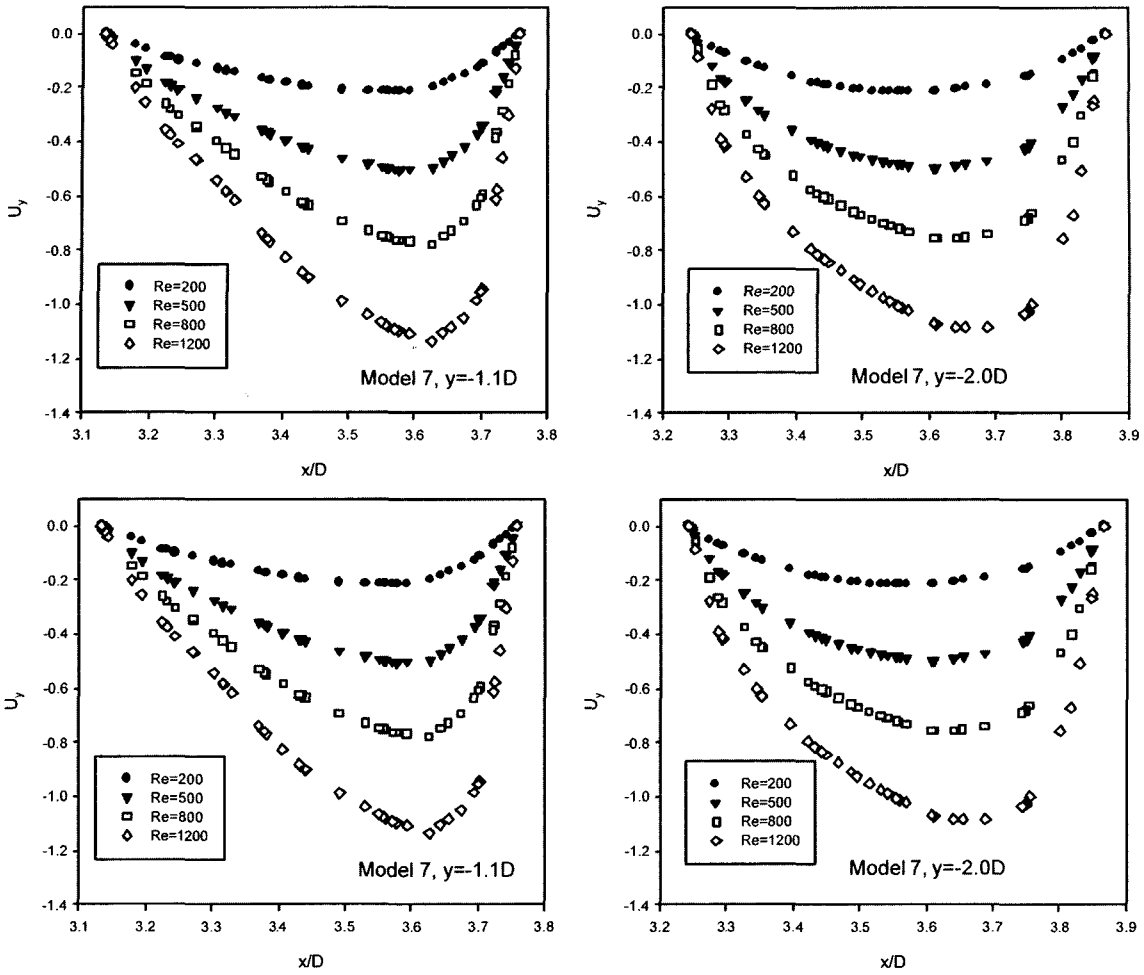

Fig. 7. The streamwise velocities in the daughter branches at $y = \pm 1.1D$ and $\pm 2.0D$ in model 2.

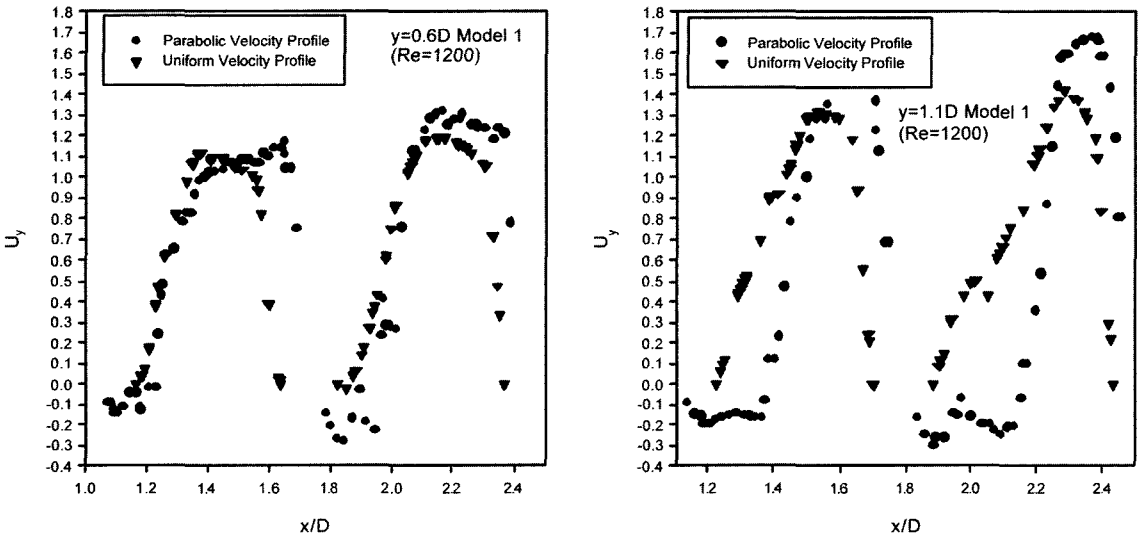

Fig. 8. Comparison of the velocity profiles at the daughter branches for two different inlet conditions in model 1.

the second branch opposite the first one. As the flow proceeds downstream in the second branch, there exists no reverse flow region and the profiles tend to shift toward the outer wall.

Fig. 8 demonstrates the results of the effect of the shape of two different inlet velocity conditions. The secondary

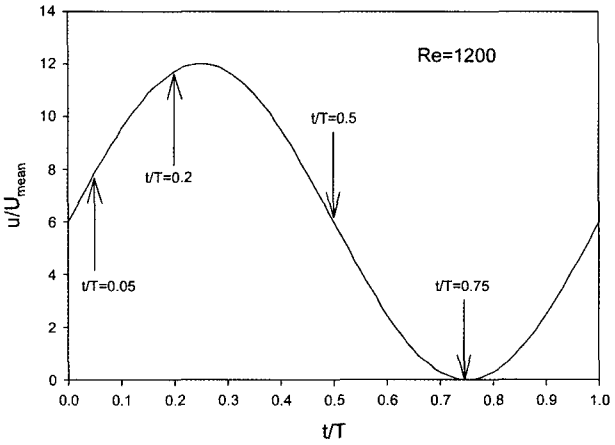

Fig. 9. Sinusoidal temporal waveform of the velocity profile at inlet region.

flows in the case of the parabolic velocity inlet condition develop along the proximal side near the celiac-superior mesentric junctions, forming and strengthening vortices as the flow proceeds downstream along the daughter branches as shown in Fig. 8.

Fig. 9 shows the sinusoidal temporal waveform of the inlet velocity. The pulse has a maximum u/U_{mean} of 12.005, minimum u/U_{mean} of 0, and the Womersley number is 2.85.

Fig. 10 depicts the velocity contours at four distinct time levels in the daughter branches of $y = 0.6D$ of model 1. As you see, negative axial velocities are observed along the proximal wall within the daughter branches. It is consistent with the presence of flow recirculation within the flow separation region discussed in the steady flow cases. Complex velocity distributions were appeared at the abdominal aortic bifurcation with the flow reversal. The secondary flow motion in the cross-section of the daughter branches consists of two counter-rotating vortices.

For pulsatile flow, the wall shear stresses in model 1 at four different points in the pulsatile cycle are presented at Fig. 11. The wall shear stresses are considerably higher along the anterior wall of the mother vessel (the wall with the branches) than along the posterior wall, opposite the celiac-superior mesenteric arteries. The wall shear stresses are higher in the immediate vicinity of the daughter branches. Within the mother vessel, the maximum shear stress occurs along the anterior wall both distal to and proximal to the branches. The peak shear stress during the input pulse occurs at $t/T = 0.2$ second.

For model 2, the wall shear stresses at equivalent time points to those of Fig. 11 are presented in Fig. 12. The peak value of wall shear stress occurs in the immediate vicinity of the first branch. The peak wall shear stress in model 2 is lower than that in model 1.

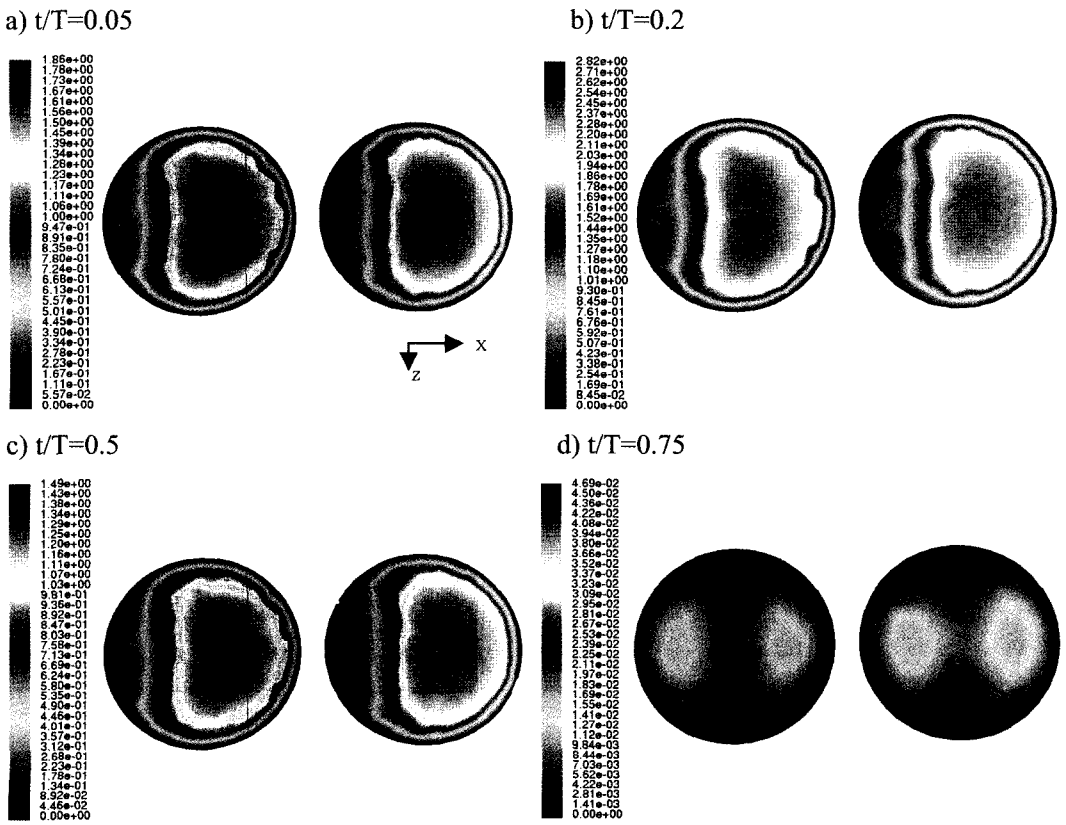

Fig. 10. The velocity contours in the daughter branches of the position at $y = 0.6D$ at four distinct time levels in model 1.

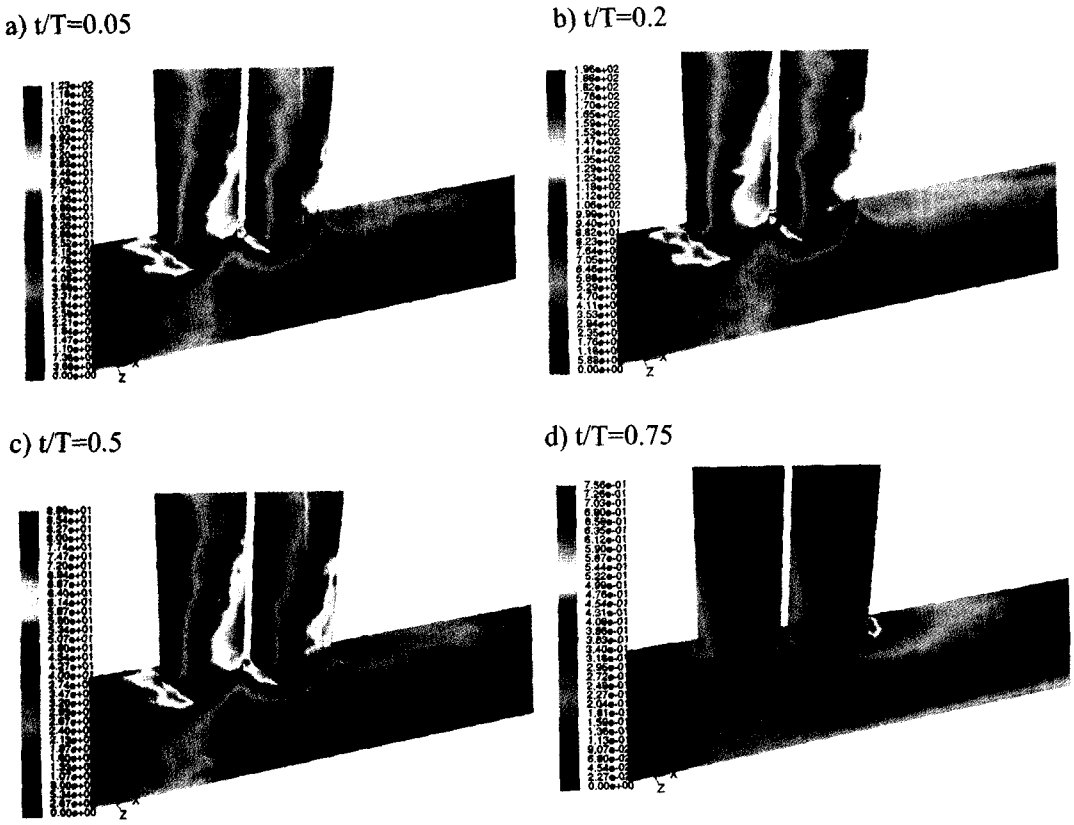

Fig. 11. Wall shear stresses at four distinct time levels in model 1.

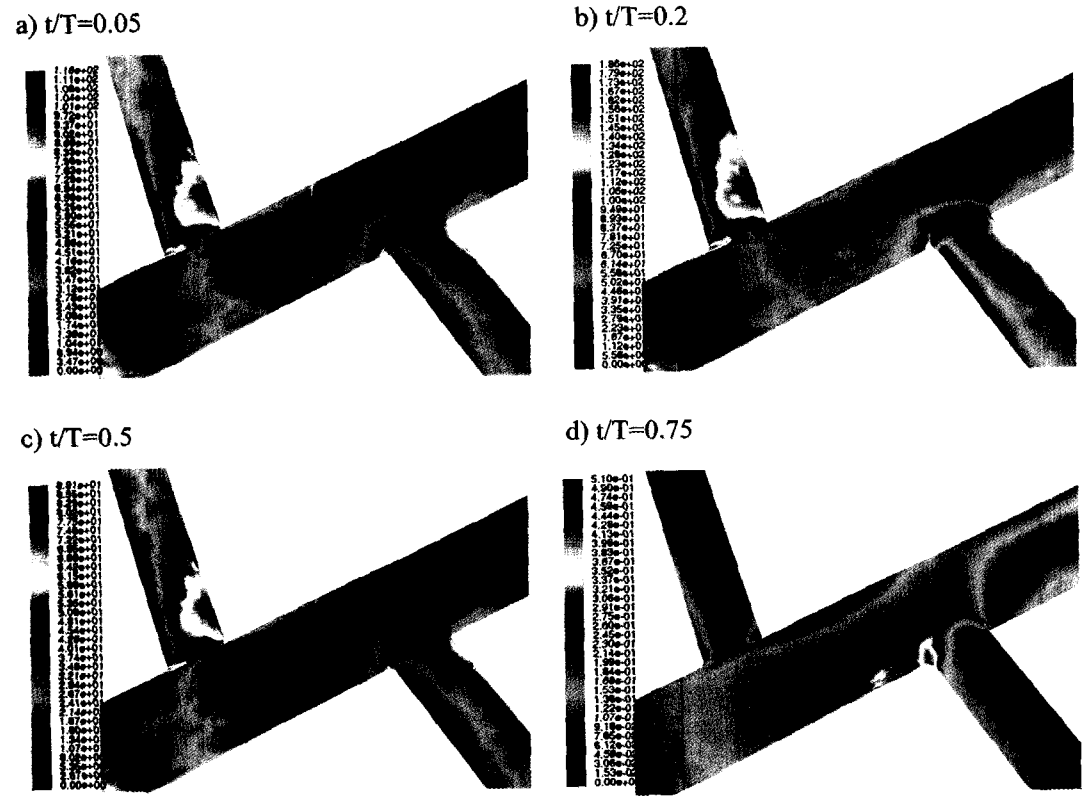

Fig. 12. Wall shear stresses at four distinct time levels in model 2.

4. Discussion and conclusions

In this study, simulations under both steady and pulsatile flow conditions were conducted to understand fluid mechanical interactions using CFD in the immediate vicinity of two large arterial branches for two models of abdominal aortic branches. However, the simulations in this study contain the realistic geometry of a rabbit, it is assumed no wall motion and the approximation has been made for the inlet and outlet flow conditions. Future studies need to improve physical approximations and models to determine the important biological significance.

The hemodynamic factors in the region of arterial branches on two different geometries play an important role on the localization of early atherosclerotic lesions. Our specific aim of this study is to understand the sensitivity of the computed flow field to prescribed changes in geometric and flow parameters. We conducted a parametric study of the effects of flow Reynolds number and the shape of the inlet velocity profile on the computed flow field. While our simulation was not direct physiological relevance, this parametric study with changes of each of these parameters provides us information of the correlation between arterial fluid dynamics and the localization of early atherosclerotic lesion at the abdominal aortic branches.

The velocity vectors with Reynolds numbers illustrate that the velocity profile within the abdominal aortic section becomes sharply skewed toward the branch sides (Fig. 4), and toward the first branch side and then skewed toward the opposite side (Fig. 6), and this skewness persisted along the abdominal aorta. The velocity profile is sharply skewed towards the distal wall and the region of recirculation zone is present within the celiac artery along the proximal wall. The significant flow separation and flow reversal occurred proximal to the aortic branches. As shown in Fig. 4 and 6, flow separation is also observed opposite the abdominal aortic branches. This occurred in the superior mesenteric artery in model 1 and in the left renal artery in model 2. Early atherosclerotic lesion primarily develops in this region where secondary flow patterns and greater shear stress gradient exists (*Barakat et al.*, 1997a).

For pulsatile flow, the wall shear stresses were generally high along the anterior wall in the vicinity of the branches and low along the posterior wall within the abdominal aorta. The wall shear stresses were considerably higher along the distal walls than along the proximal walls. The preferential development of the atherosclerotic lesion can occur in region of either maxima or minima in wall shear stress.

The results of the computations have revealed some general flow phenomena that include the following:

a) In model 1, the velocity profiles within the branches for higher Reynolds number are M-shaped due to the strong skewness.
b) In model 2, the loss of momentum due to the turning effects at the first branch leads to the absence of a reversed flow region at the entrance region of the second branch.
c) The peak value of wall shear stress is generally highest in the immediate vicinity of the branches (both proximal and distal). The peak wall shear stress in model 2 is lower than that in model 1.
d) Although quantitative comparisons of our results with the physiological data have not been possible, our results provide useful information for the localization of early atherosclerotic lesions.

Acknowledgements

This work was supported by the Special Research Fund of Andong National University and Brain Korea 21.

References

Barakat, A.I., T. Karino and C.K Colton, 1997a, Microcinematographic studies of flow patterns in the excised rabbit aorta and its major branches, *Biorheology* **34**, 195-221.

Barakat, A.I., T. Karino, R.P. Marini and C.K Colton, 1997b, Measurement of flow rates through aortic branches in the anesthetized rabbits, *Lab. Animal Science* **47**, 184-189.

Buchanan, J.R., C. Kleinstreuer, S. Hyun and G.A. Truskey, 2003, Hemodynamics simulation and identification of susceptible sites of atherosclerotic lesion formation in a model abdominal aorta, *J. of Biomechnaincs* **36**, 1185-1196.

Cheer, A.Y., H.A. Dwyer, A.I. Barakat, E. Sy and M. Bice, 1998, Computational study of the effect of geometric and flow parameters on the steady flow field at the rabbit aorto-celiac bifurcation, *Biorheology* **35**, 415-435.

Karino, T., H.M. Herman and L. Goldsmith, 1979, Particle flow behavior in models of branching vessels: I. vortices in 90° T-junctions, *Biorheology* **16**, 231-248.

Lei, M., C. Kleinstreuer and G.A. Truskey, 1998, Numerical investigation and prediction of atherogenic sites in branching arteries, *J. of Biomechanical Eng.* **117**, 350-357.

Seo, T.W., L.G. Schachter and A.I. Barakat, 2004, Computational study of fluid mechanical disturbance induced by endovascular stents, *Annals of Biomedical Eng.*, under Review.

Shipkowitz, T., V.G.J. Rodgers, L.J. Franzin and K.B. Chandran, 2000, Numerical study on the effect of secondary flow in the human aortic branches, *J. of Biomechanics* **33**, 717-728.

Taylor, C.A., T.J.R. Hughes and C.K. Zarins, 1998, Finite element modeling of three-dimensional pulsatile flow in the abdominal aorta: relevance to atherosclerosis, *Annals of Biomedical Eng.*, **26**, 975-987.